energies

MDPI

Article

An Algorithm for Circuit Parameter Identification in Lightning Impulse Voltage Generation for Low-Inductance Loads

Piyapon Tuethong, Krit Kitwattana, Peerawut Yutthagowith * and Anantawat Kunakorn

Faculty of Engineering, King Mongkut's Institute of Technology Ladkrabang, Bangkok 10520, Thailand; t_piyapon@hotmail.com (P.T.); highvoltage.eg@gmail.com (K.K.); anantawat.ku@kmitl.ac.th (A.K.)

* Correspondence: kypeeraw@kmitl.ac.th; Tel.: +66-(0)2-329-8330

Received: 28 June 2020; Accepted: 23 July 2020; Published: 31 July 2020

Abstract: This paper presents an effective technique based on an artificial neural network algorithm utilized for circuit parameter identification in lightning impulse generation for low inductance loads such as low voltage windings of a power transformer, a large distribution transformer and an air core reactor. The limitation of the combination between Glaninger's circuit and the circuit parameter selection from Feser's suggestions in term of producing an impulse waveform to be compliant with standard requirements when working with a low inductance load is discussed. In Feser's approach, the circuit parameters of the generation circuit need to be further adjusted to obtain the waveform compliant with the standard requirement. In this process, trial and error approaches based on test engineers' experience are employed in the circuit parameter selection. To avoid the unintentional damage from electrical field stress during the voltage waveform adjustment process, circuit simulators, such as Pspice and EMTP/ATP, are very useful to examine the generated voltage waveform before the experiments on the test object are carried out. In this paper, a system parameter identification based on an artificial neural network algorithm is applied to determine the appropriate circuit parameters in the test circuit. This impulse voltage generation with the selected circuit parameters was verified by simulations and an experiment. It was found that the generation circuit gives satisfactory impulse voltage waveforms in accordance with the standard requirement for the maximum charging capacitance of 10 μF and the load inductance from 400 μH to 4 mH. From the simulation and experimental results of all cases, the approach proposed in this paper is useful for test engineers in selection of appropriate circuit components for impulse voltage tests with low inductance loads instead of employing conventional trial and error in circuit component selection.

Keywords: artificial neural network; circuit design; Glaninger circuit; lightning impulse voltage tests; low inductance loads; system parameter identification

1. Introduction

Lightning is a crucial cause of insulation failure in a high voltage system. It is necessary to examine insulation performance of high voltage equipment with high voltage withstand tests [1,2] before installation at the workplace. The standard lightning impulse voltage waveform [1] is defined by the peak voltage (V_p), the front-time (T_1) and the time to half (T_2). In Figure 1, the lightning impulse voltage in the HV test is generated by Marx's circuit [3], of which circuit components are a charging capacitor (C_s), a spark gap (G), a front-time resistor (R_d), a tail-time resistor (R_e) and a load capacitor (C_b) (a tested object with a high voltage measuring system).

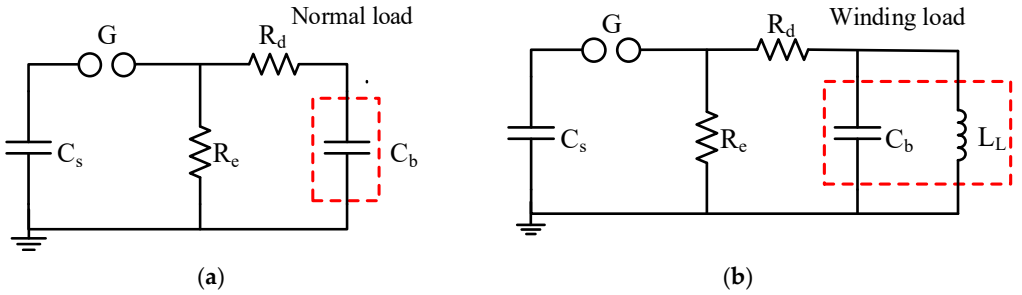

Figure 1. Conventional Marx's circuit with different loads for generation of impulse voltage; (**a**) normal load; and (**b**) winding load.

Normally, a usual load of the impulse voltage generation can be represented adequately by only a capacitor. When the efficiency of the generation is given, the voltage peak can be controlled by a charging voltage. The front-time (T_1) is controlled by a front-time resistance (R_d) and a load capacitance (C_b) as in Equation (1) [3], and the time to half (T_2) is controlled by a tail-time resistance (R_e) and a charging capacitance (C_s) as in Equation (2) [3]. The front-time and the time to half with the tolerances of the standard lightning impulse voltage are equal to 1.2 µs ±30% (0.84–1.56 µs) and 50 µs ±20% (40–60 µs), respectively.

$$T_1 = 2.96R_d\frac{C_bC_s}{C_b + C_s} \quad (1)$$

$$T_2 = 0.73R_e(C_b + C_s) \quad (2)$$

When performing a lightning impulse voltage test on the low inductance load, for example a low voltage winding of a power transformer and a reactor [4–7], the conventional impulse voltage generation Marx's circuit occasionally cannot produce the voltage waveform in accordance with the standard requirement [8,9]. The equivalent circuit of these loads can be represented well with an inductor connected in parallel with a capacitor, as shown in Figure 1b. These low inductance loads lead the time to half being shorter than 40 µs. In the case of a normal load, the time to half of the waveform generated using the conventional Marx's circuit can be expanded by increasing R_e and/or C_s. However, for a low inductance load, increasing R_e is not applicable practically [8]. To increase C_s, in each stage of an impulse, the generator must consist of several charging capacitors which have to be connected in parallel. Normally, the maximum charging capacitance is limited to 10–20 µF which is equivalent to the total capacitance of 5–10-stage charging capacitors in parallel connection. Such a configuration of the impulse generator is not applicable in design and construction. Therefore, adjustment of R_e and C_s is not an exact solution for increasing the time to half in the case of the low inductance load.

For better understanding, example cases, in which the equivalent circuit of a winding load is represented by an inductor (L_L = 2 mH) connected in parallel with the capacitor (C_b = 4 nF), are considered. Using the conventional circuit shown in Figure 1b, the circuit parameters were selected on the basis of Equations (1) and (2). For simplification and comparison of the circuit efficiencies of the considered circuits, the charging voltage was set to be 1 per unit. With the selected circuit parameters, the generated waveforms computed by the circuit simulator (EMTP/ATP) shown in Figure 2 were evaluated according to the standard [10–12] based on the two-exponential function curves and the k-factor filter. Using the conventional Marx's circuit, in Case 1, the charging capacitor was set to 2 µF, and the front-time resistance (R_d) of 100 Ω was selected by Equation (1). The tail-time resistance (R_e) of 45 Ω was selected by Equation (2). The time to half of the generated waveform is only 12.16 µs. To increase the time to half, the tail-time resistance (R_e) needs to be increased. In Case 2, the tail-time resistor was not connected in the circuit ($R_e = \infty$), and the time to half of the generated waveform is still of only 15.15 µs, which is shorter than the standard requirement. The selected circuit parameters and the evaluated waveform parameters are shown in Table 1.

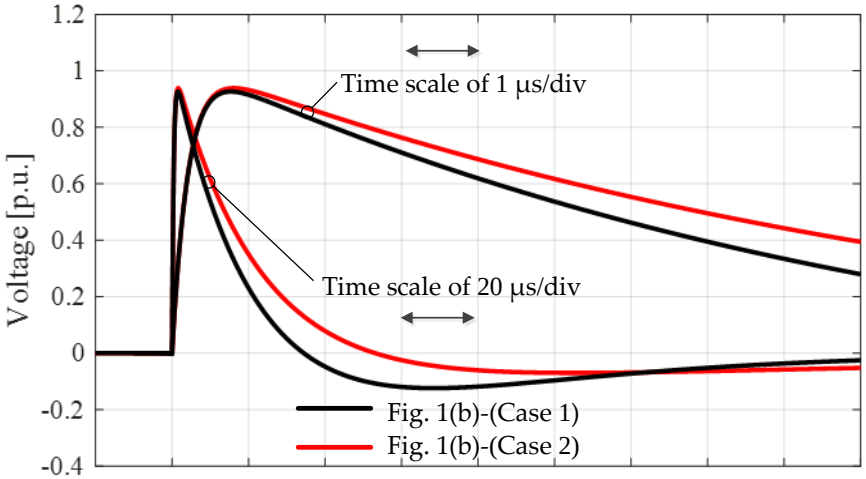

Figure 2. Generated waveforms using the conventional circuit.

Table 1. Circuit parameters in the conventional lightning impulse voltage generation circuits and waveforms parameters of the generated waveforms.

Waveform Parameters	Circuit Cases	
	Figure 1b (Case 1)	**Figure 1b (Case 2)**
Efficiency	92.63%	93.86%
Overshoot rate (<5%)	−0.69% (✓)	−0.40% (✓)
Undershoot rate (<50%)	13.3% (✓)	7.29% (✓)
T_1 (0.84–1.56 μs)	1.05 μs (✓)	1.08 μs (✓)
T_2 (40–60 μs)	12.16 μs **(✕)**	15.15 μs **(✕)**

✓ indicates the parameters being in accordance with the standard requirement [4,5]; ✕ indicates the parameters not being in accordance with the standard requirement [4,5].

To overcome this problem, Glaninger's circuit in Figure 3 was proposed in 1975 [8]. The parallel connection of the additional inductor (L_d) with the front-time resistor (R_d) is used. This is for the purpose of the short circuit condition during the tail time (after the time to crest) as the time to half can be extended. The parallel connection of the additional parallel resistor (R_p) with the test object is used for controlling the overshoot rate of the generated waveform. In 1978, K. Feser [13] proposed the approach for selection of the appropriate circuit parameters, i.e., the charging capacitance (C_s), the front-time resistance (R_d), the additional inductance (L_d) and the additional parallel resistance (R_p), as given in Equations (3)–(6). In addition, the appropriate tail-time resistor (R_e) has to be selected to obtain the undershoot voltage being less than 50% of the peak voltage [5,6].

$$C_s \approx T_2^2 / L_L \tag{3}$$

$$R_d = \left(0.4 \times 10^{-6}\right) / C_b \tag{4}$$

$$L_d = 1.25 \times 10^{-6} R_d \tag{5}$$

$$R_p = (R_d L_L) / L_d \tag{6}$$

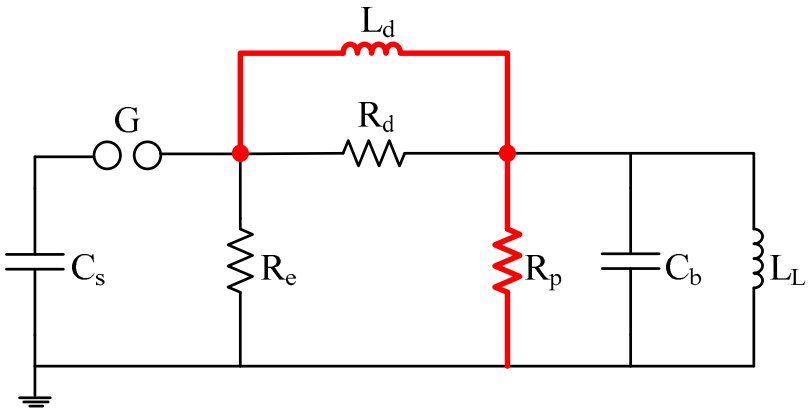

Figure 3. Glaninger's circuit with a winding load for the impulse voltage generation.

However, the distortion in the waveform generated by the circuit with parameters from K. Feser's suggestion was noticed. A trial and error approach, then, is recommended to adjust the circuit parameters to mitigate the waveform distortion and to obtain the waveform parameters according to the standard requirement.

For better understanding, the Glaninger's circuit shown in Figure 3 with K. Feser's approach was utilized to generate a lightning impulse voltage waveform on the same load in the previous cases (L_L = 2 mH and C_b = 4 nF). The time to half was set to 60 µs. Based on Equations (3)–(5), L_d and R_p were calculated as 125 µH and 1600 Ω, respectively. It was found that the front-time of the generated waveform computed by the circuit simulator (EMTP/ATP) in Figure 4 complies with the standard requirement, but the time to half is shorter than the standard requirement and the overshoot rate of 8.12% is higher than the value defined by the standard as 5% [5,6]. Figure 4 shows that, when L_d and R_p are changed, the reduction of overshoot is noticed. These L_d and R_p are 100 µH and 310 Ω, respectively, instead of 125 µH and 1600 Ω calculated using Equations (4) and (5). It is recommended that the combination of Glaninger's circuit with K. Feser's suggested equations has to be modified so that the proper impulse voltage waveform can be achieved when dealing with low inductance loads. The circuit parameters and the waveform parameters were selected and evaluated, as given in Table 2.

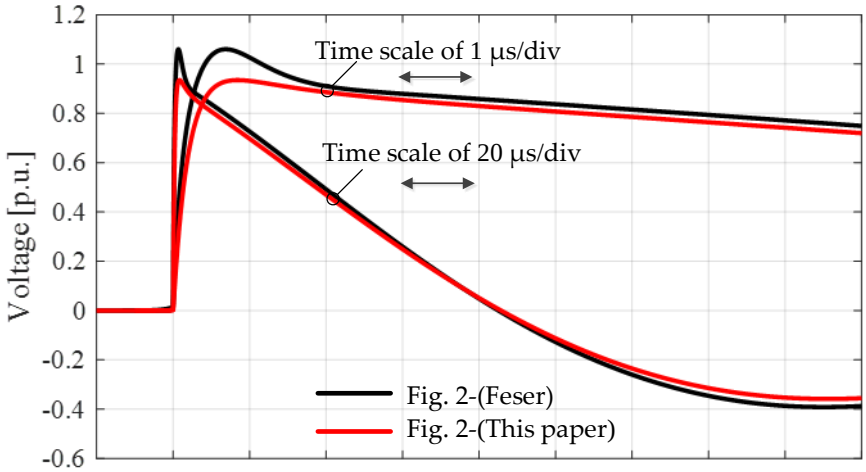

Figure 4. Comparison of generated waveforms by Glaninger's circuits.

Table 2. Circuit parameters in the Glaninger's generation circuits and waveforms parameters of the generated waveforms.

Circuit and Time Parameters	Circuit Cases	
	Figure 2 (K. Feser)	**Figure 2 (This Paper)**
L_L	2.0 mH	2.0 mH
C_b	4.0 nF	4.0 nF
C_s	2.0 µF	2.0 µF
R_d	100 Ω	120 Ω
L_d	125 µH	100 µH
R_p	1600 Ω	310 Ω
R_e	52.2 Ω	58.3 Ω
Efficiency	106.03%	98.75%
Overshoot rate (<5%)	+8.12% (✗)	+1.33% (✓)
Undershoot rate (<50%)	38.09% (✓)	41.04% (✓)
T_1 (0.84–1.56 µs)	0.986 µs (✓)	1.16 µs (✓)
T_2 (40–60 µs)	37.70 µs (✗)	41.14 µs (✓)

✓ indicates the parameters being in accordance with the standard requirement. [4,5] ✗ indicates the parameters not being in accordance with the standard requirement. [4,5].

In fact, there are other approaches [14,15] for the circuit parameter selection in the lightning impulse voltage test on the low inductance load. The characteristics of the loads under test in the frequency domain are extracted, and trial and error approaches for the circuit parameter selection based on computer simulation are still utilized to obtain the test voltage waveform according to the standard requirement. Therefore, it is not convenient for test engineers in the real practice.

It has been shown that the operation of an impulse generation circuit with a low inductance load requires specific attention in component parameters selection. Therefore, this paper aims to propose a convenient and simple approach based on an artificial neural network algorithm in the selection of parameters and components of Glaninger's impulse voltage generation circuit. With the selected components, the generated waveform has less distortion. The efficiency is over 60%, and the undershoot voltage is about 40%. With the maximum charging capacitance of 10 µF, the test object inductance of 400 µH can be tested by this design circuit. The design procedure validity was confirmed by some simulation and experiments in a high voltage laboratory.

2. Proposed Approach for Parameter Selection of the Lightning Impulse Voltage Generation for Low Inductance Loads

In this paper, a system parameter identification based on an artificial neural network (ANN) is adopted to determine the circuit component parameters of the specific lightning impulse voltage generation circuit for low inductance loads of the inductance being in the range of 0.4 mH ≤ L_L ≤ 4 mH [10,16]. The ANN approach is very effective and utilized instead of a trial and error method with test engineers' experiences. The multi-layer feed-forward ANN with a backpropagation learning algorithm is selected for the system parameter identification model in this paper, and the simplest structure with the fewest layers and neurons is considered.

For the ANN parameter identification, input and output parameters are required. The input parameters of the model are load inductance (L_L) and capacitance (C_b) of the test object, while the output parameters are the circuit component parameters of the generation circuit, i.e., the charging capacitance (C_s), the front-time resistance (R_d), the additional inductance (L_d), the additional parallel resistance (R_p) and the time to half resistance (R_e).

In the training process, 30 cases of the generation circuits with the input parameters (load inductance from 0.4 to 4 mH and capacitance from 1 to 10 nF) were utilized. All generated waveforms were computed by EMTP/ATP, and the waveform parameters were evaluated according to the IEC standards [1,10–12]. Firstly, as shown in Table 3, the output parameters, i.e., C_s, R_d, L_d, R_p and R_e, were calculated by Feser's approach. Then, such output parameters of each case were adjusted to achieve the criteria of the standard waveform parameter requirements, i.e., the front time of about 1.2 μs, the time to half of not less than 40 μs, the overshoot rate of less than 5%, the undershoot rate of about 40% and circuit efficiency (the ratio of the charging voltage and the generated peak voltage) of higher than 60%. The input parameter and the adjusted output parameters shown in Table 4 were set to be training data, while the evaluated waveform parameters associated with the input and output parameters are given in Table 5.

Table 3. Circuit component parameters calculated by Feser's approach.

Case No.	Circuit Component Parameters						
	L_L (mH)	C_b (nF)	C_s (μF)	R_d (Ω)	L_d (mH)	R_p (Ω)	R_e (Ω)
1	0.4	1.0	9.0	400	0.5	320.00	16.00
2	0.8	1.0	5.0	400	0.5	640.00	25.80
3	1.0	1.0	4.0	400	0.5	800.00	31.00
4	2.0	1.0	2.0	400	0.5	1600.00	56.60
5	3.0	1.0	1.5	400	0.5	2400.00	77.30
6	4.0	1.0	1.0	400	0.5	3200.00	107.00
7	0.4	2.0	9.0	200	0.25	320.00	13.60
8	0.8	2.0	5.0	200	0.25	640.00	23.20
9	1.0	2.0	4.0	200	0.25	800.00	28.30
10	2.0	2.0	2.0	200	0.25	1600.00	53.70
11	3.0	2.0	1.5	200	0.25	2400.00	74.50
12	4.0	2.0	1.0	200	0.25	3200.00	104.00
13	0.4	4.0	9.0	100	0.125	320.00	12.20
14	0.8	4.0	5.0	100	0.125	640.00	21.80
15	1.0	4.0	4.0	100	0.125	800.00	26.80
16	2.0	4.0	2.0	100	0.125	1600.00	52.20
17	3.0	4.0	1.5	100	0.125	2400.00	73.00
18	4.0	4.0	1.0	100	0.125	3200.00	103.00
19	0.4	8.0	9.0	50	0.0625	320.00	11.50
20	0.8	8.0	5.0	50	0.0625	640.00	21.00
21	1.0	8.0	4.0	50	0.0625	800.00	26.10
22	2.0	8.0	2.0	50	0.0625	1600.00	51.40
23	3.0	8.0	1.5	50	0.0625	2400.00	72.30
24	4.0	8.0	1.0	50	0.0625	3200.00	102.00
25	0.4	10.0	9.0	40	0.05	320.00	11.30
26	0.8	10.0	5.0	40	0.05	640.00	20.90
27	1.0	10.0	4.0	40	0.05	800.00	25.90
28	2.0	10.0	2.0	40	0.05	1600.00	51.20
29	3.0	10.0	1.5	40	0.05	2400.00	72.10
30	4.0	10.0	1.0	40	0.05	3200.00	102.00

Table 4. The adjusted circuit component parameters of the generation circuit used as training data.

Case No.	Circuit Component Parameters						
	L_L (mH)	C_b (nF)	C_s (μF)	R_d (Ω)	L_d (mH)	R_p (Ω)	R_e (Ω)
1	0.4	1.0	9.0	1000	0.25	382.43	12.75
2	0.8	1.0	5.0	700	0.25	523.82	21.74
3	1.0	1.0	4.0	650	0.25	573.47	26.52
4	2.0	1.0	2.0	550	0.25	728.40	53.67
5	3.0	1.0	1.5	500	0.25	818.94	79.13

Table 4. *Cont.*

Case No.	Circuit Component Parameters						
	L_L (mH)	C_b (nF)	C_s (μF)	R_d (Ω)	L_d (mH)	R_p (Ω)	R_e (Ω)
6	4.0	1.0	1.0	500	0.25	861.40	117.35
7	0.4	2.0	9.0	400	0.15	266.17	11.73
8	0.8	2.0	5.0	300	0.15	356.03	20.68
9	1.0	2.0	4.0	300	0.15	380.73	25.43
10	2.0	2.0	2.0	250	0.15	471.13	59.02
11	3.0	2.0	1.5	250	0.15	504.20	82.49
12	4.0	2.0	1.0	250	0.15	522.66	128.84
13	0.4	4.0	9.0	150	0.10	187.94	11.18
14	0.8	4.0	5.0	130	0.10	245.45	20.12
15	1.0	4.0	4.0	130	0.10	261.70	26.53
16	2.0	4.0	2.0	120	0.10	310.07	58.33
17	3.0	4.0	1.5	120	0.10	328.52	90.92
18	4.0	4.0	1.0	120	0.10	338.63	140.87
19	0.4	8.0	9.0	60	0.10	123.14	11.18
20	0.8	8.0	5.0	55	0.10	172.79	20.12
21	1.0	8.0	4.0	50	0.10	186.83	26.53
22	2.0	8.0	2.0	50	0.10	237.47	58.32
23	3.0	8.0	1.5	50	0.10	261.17	90.92
24	4.0	8.0	1.0	50	0.10	274.91	140.87
25	0.4	10.0	9.0	50	0.05	111.69	12.02
26	0.8	10.0	5.0	50	0.05	135.48	23.47
27	1.0	10.0	4.0	45	0.05	145.30	29.16
28	2.0	10.0	2.0	45	0.05	161.40	70.43
29	3.0	10.0	1.5	45	0.05	167.62	112.73
30	4.0	10.0	1.0	43	0.05	173.84	222.74

Table 5. The generated waveform parameters associated with the cases in Table 4.

Case No.	Waveform Parameters				
	Efficiency (%)	T_1 (μs)	T_2 (μs)	Overshoot (%)	Undershoot (%)
1	64.39	1.04	47.11	+2.81	39.50
2	79.88	1.03	44.35	+2.83	39.15
3	83.97	1.03	43.15	+2.96	38.98
4	93.59	1.03	41.56	+3.08	39.98
5	97.20	1.02	43.96	+2.82	41.06
6	99.25	1.02	41.38	+2.98	41.58
7	76.02	1.11	43.25	+2.60	39.26
8	88.15	1.10	42.02	+2.64	38.81
9	91.29	1.11	41.02	+3.02	38.38
10	97.50	1.08	42.14	+2.20	42.21
11	100.00	1.09	43.38	+2.57	41.10
12	101.35	1.10	41.33	+2.62	42.17
13	82.69	1.16	41.53	+1.29	39.37
14	91.96	1.16	40.95	+1.43	38.53
15	94.34	1.17	41.28	+1.55	39.79
16	98.75	1.16	41.14	+1.33	41.04
17	100.58	1.17	43.79	+1.41	41.90
18	101.30	1.17	41.05	+1.52	41.72
19	79.74	1.17	42.64	−2.26	40.11
20	89.12	1.25	41.81	−1.43	38.95
21	90.86	1.20	42.29	−1.95	40.36
22	94.78	1.16	42.00	−2.36	41.33
23	96.43	1.18	44.48	−2.30	41.82

Table 5. *Cont.*

Case No.	Waveform Parameters				
	Efficiency (%)	T_1 (μs)	T_2 (μs)	Overshoot (%)	Undershoot (%)
24	96.94	1.18	41.66	−2.19	41.52
25	91.16	1.19	41.17	+0.13	41.99
26	96.92	1.24	41.99	+0.60	41.78
27	97.45	1.18	41.53	+0.02	41.31
28	99.87	1.19	41.35	+0.20	41.81
29	100.85	1.20	43.22	+0.48	41.18
30	100.83	1.20	41.04	+0.37	41.62

In the testing process, 11 cases, which are different from the cases in the training process, were selected. The results of the testing process are presented in Section 3.

From many efforts of the construction of the ANN models based on the concerns of simplicity, the model has three layers: an input layer with two neurons, a hidden layer with four neurons and an output layer with one neuron. The structure of the developed ANN models and the mathematical function of a neuron consisting of weighting, summation, biasing and activating by an activation function are depicted in Figures 5 and 6, respectively [17].

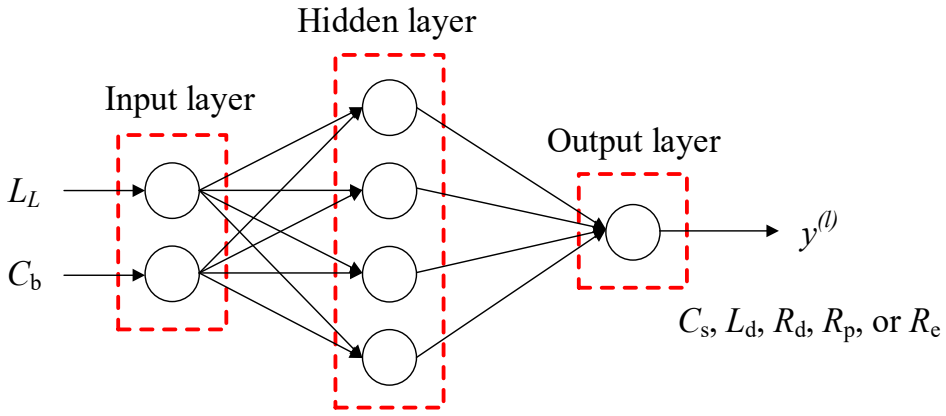

Figure 5. The ANN model used in the circuit parameter selection.

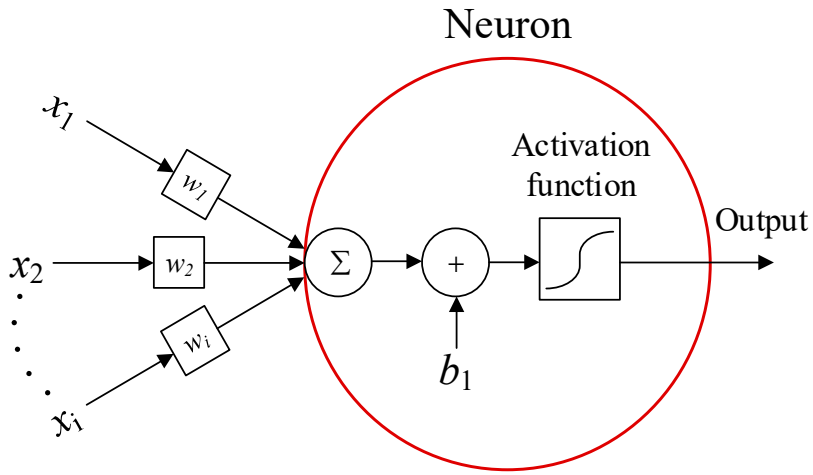

Figure 6. Mathematical function of a neuron in an ANN model.

The training process for obtaining the model parameters is presented in Figure 7. The maximum deviations of the determined output parameters were set as 5%. A more complicated model with a higher accuracy could be developed using a similar ANN approach, but the simplification is concerned so that the model can be readily transferred into a matrix form and easily implemented for the software development.

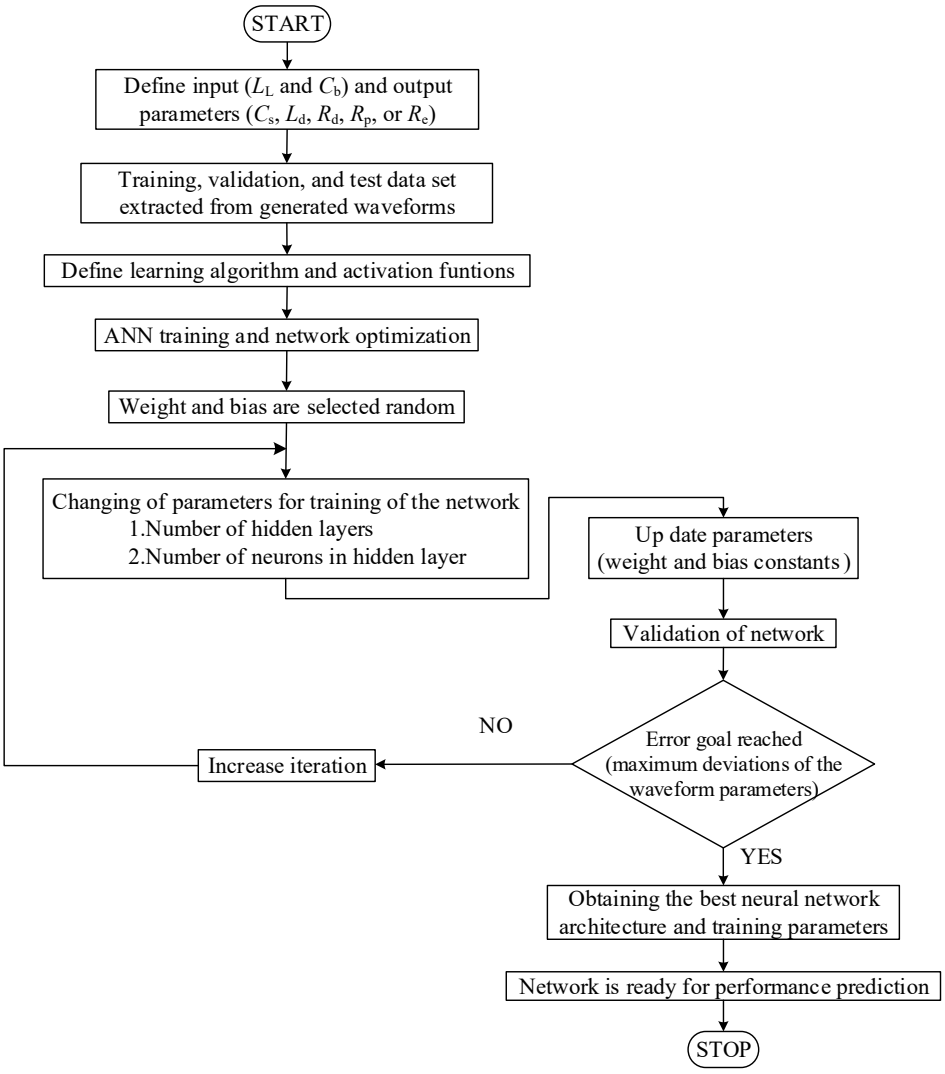

Figure 7. Flowchart of an ANN training.

For simplicity and reduction of the model dimension, weighting and bias constants of the output layer are transferred to include the weighting and bias constants of the hidden layer. Therefore, the predicted output parameters from the developed model can be calculated by Equation (7), where x_i is input parameters, i.e., L_L, and C_b. $y^{(l)}$ (C_s, L_d, R_d, R_p, or R_e) is a predicted parameter of (l). $w_{1,ij}^{(l)}$ and $b_{1,ij}^{(l)}$ are weighting and bias constants of the input layer associated with an input parameter of i and a neuron of j of the hidden layer, respectively. $w_{2,j}^{(l)}$ and $b_{2,j}^{(l)}$ are weighting and bias parameters of the hidden layer associated with neuron of j of the hidden layer, respectively. $f(\cdot)$ is a selected activation function being a tansig function as given in Equation (8).

$$y^{(l)} = \sum_{j=1}^{n}\left\{w_{2,j}^{(l)} f\left(\sum_{i=1}^{N}\left(w_{1,ij}^{(l)} \cdot x_i + b_{1,ij}^{(l)}\right)\right) + b_{2,j}^{(l)}\right\} \quad (7)$$

$$f(x) = \frac{2}{1 + e^{-2x}} - 1 \tag{8}$$

For convenience in calculation and software development, Equation (7) can be rewritten in the matrix form as Equation (9), where X is input parameter in a matrix form. $W_1^{(l)}$ and $B_1^{(l)}$ are a weighting matrix and a bias vector of the input layer, respectively. $W_2^{(l)}$ and $B_2^{(l)}$ are a weighting matrix and a bias vector of the hidden layer, respectively.

$$y^{(l)} = W_2^{(l)}\left\{f\left(W_1^{(l)}X + B_1^{(l)}\right)\right\} + B_2^{(l)} \tag{9}$$

The values of $W_1^{(l)}$, $W_2^{(l)}$, $B_1^{(l)}$ and $B_2^{(l)}$ are given as Equations (10)–(13).

$$\begin{gathered} W_1^{(C_s)} = \begin{bmatrix} 1.58*10^9 & 3.53*10^3 \\ -1.75*10^9 & 2.86*10^3 \\ -1.27*10^6 & -1.05*10^3 \\ 5.71*10^4 & -1.11*10^3 \end{bmatrix}, W_1^{(R_d)} = \begin{bmatrix} -7.20*10^8 & -1.64*10^3 \\ -5.89*10^8 & 2.03*10^1 \\ -6.24*10^8 & -3.49*10^1 \\ 7.32*10^7 & 1.01*10^3 \end{bmatrix} \\ W_1^{(R_e)} = \begin{bmatrix} 5.64*10^8 & 9.59*10^3 \\ 1.34*10^9 & 7.03*10^2 \\ 2.19*10^8 & 8.70*10^2 \\ -1.34*10^7 & 5.52*10^2 \end{bmatrix}, W_1^{(R_p)} = \begin{bmatrix} 7.58*10^7 & 7.54*10^2 \\ -1.10*10^9 & 3.66*10^2 \\ -5.28*10^8 & 4.35*10^1 \\ -9.19*10^8 & -4.59*10^2 \end{bmatrix} \\ W_1^{(L_d)} = \begin{bmatrix} 7.34*10^8 & 3.59*10^{-6} \\ -7.06*10^8 & -1.83*10^{-3} \\ -3.89*10^8 & -6.68*10^2 \\ -7.92*10^8 & 3.29*10^{-5} \end{bmatrix} \end{gathered} \tag{10}$$

$$\begin{gathered} W_2^{(C_s)} = \begin{bmatrix} 0.00126 & 0.00119 & 0.51532 & 25.77544 \end{bmatrix} \\ W_2^{(R_d)} = \begin{bmatrix} 1.38668 & 0.03546 & 1.12267 & -0.2058 \end{bmatrix} \\ W_2^{(R_e)} = \begin{bmatrix} 18.77705 & 150.80452 & 8.84285 & 52.80142 \end{bmatrix} \\ W_2^{(R_p)} = \begin{bmatrix} 5.21445 & 0.67670 & 14.84922 & -6.12052 \end{bmatrix} \\ W_2^{(L_d)} = \begin{bmatrix} -0.56974 & -0.04715 & 8.32*10^8 & 1.48175 \end{bmatrix} \end{gathered} \tag{11}$$

$$\begin{gathered} B_1^{(C_s)} = \begin{bmatrix} -26.5607 \\ 8.6811 \\ 3.4238 \\ -0.4715 \end{bmatrix} B_1^{(R_d)} = \begin{bmatrix} 0.4626 \\ 3.4320 \\ -0.0231 \\ 0.8704 \end{bmatrix} \\ B_1^{(R_e)} = \begin{bmatrix} -39.0820 \\ -16.7314 \\ -3.3183 \\ -0.8408 \end{bmatrix} B_1^{(R_p)} = \begin{bmatrix} 0.3387 \\ 8.1698 \\ -0.3721 \\ 0.1272 \end{bmatrix} \\ B_1^{(L_d)} = \begin{bmatrix} -7.3558 \\ 3.9576 \\ 2.2443 \\ 0.8289 \end{bmatrix} \end{gathered} \tag{12}$$

$$\begin{gathered} B_2^{(C_s)} = 27.1046 \\ B_2^{(R_d)} = 2.7945 \\ B_2^{(R_e)} = 220.6589 \\ B_2^{(R_p)} = 5.8764 \\ B_2^{(L_d)} = 1.9233 \end{gathered} \tag{13}$$

3. Verification of Proposed Approach

To confirm the validity of the proposed design procedure, simulations and experiments were carried out and compared. The equivalent circuit parameters of winding loads and the designed circuit parameters are expressed in Table 6. It is noted that the load circuit parameters in this section are different from those of the data used in the training process. In Table 7, the generated waveform parameters associated with the cases in Table 6 are presented. Cases 1–11 are the simulation cases when load inductances are varied from 0.4 to 4 mH.

Table 6. Circuit component parameters of the generation circuit used for the validation of the developed model.

Case No.	Circuit Component Parameters						
	L_L (mH)	C_b (nF)	C_s (μF)	R_d (Ω)	L_d (mH)	R_p (Ω)	R_e (Ω)
1	0.5	1.0	8.0	893.00	0.25	423.0	14.80
2	0.5	2.0	8.0	365.00	0.15	291.0	14.30
3	0.5	4.0	8.0	140.00	0.10	204.0	13.50
4	0.5	8.0	8.0	57.20	0.10	139.6	13.00
5	0.5	10.0	8.0	50.40	0.05	117.3	14.70
6	0.4	8.5	9.0	56.00	0.094	110.0	10.90
7	0.5	8.5	8.0	54.30	0.094	120.8	13.10
8	0.8	8.5	5.0	51.04	0.094	146.8	20.49
9	1.0	8.5	4.0	49.70	0.094	160.0	26.27
10	2.0	8.5	2.0	47.47	0.094	201.5	61.47
11	4.0	8.5	1.0	47.36	0.094	255.6	143.96

Table 7. The generated waveform parameters associated with the cases in Table 6.

Case No.	Waveform Parameters				
	Efficiency (%)	T_1 (μs)	T_2 (μs)	Overshoot (%)	Undershoot (%)
1	69.68	1.03	48.19	+2.43	40.11
2	80.50	1.12	45.35	+2.41	40.75
3	86.02	1.16	43.53	+0.94	40.30
4	83.28	1.16	43.77	−2.09	39.82
5	93.19	1.23	43.43	−0.03	42.80
6	79.46	1.21	42.55	−3.30	39.90
7	82.54	1.22	44.47	−3.49	40.63
8	87.65	1.22	42.74	−3.38	39.97
9	89.58	1.21	42.54	−3.37	40.37
10	93.92	1.20	42.67	−3.26	42.15
11	96.89	1.19	41.51	−2.24	41.24

In these cases, the charging voltages were set to be 1 per unit for the case of simplicity and for the purpose of comparison of the circuit efficiencies. Figures 8–12 show the examples of the generated impulse voltage waveforms by the proposed approach.

In addition to 11 cases as described above, two further cases were considered. These cases (Cases 12 and 13) are the only cases which represent the comparison between simulation and experimental results. In these cases, two low voltage inductors used in a harmonic filter system were employed as a load under tests. The load inductances (L_L) were 2.013 and 1.308 mH. The load capacitances were less than 10 pF, so additional capacitances were added in the test circuit.

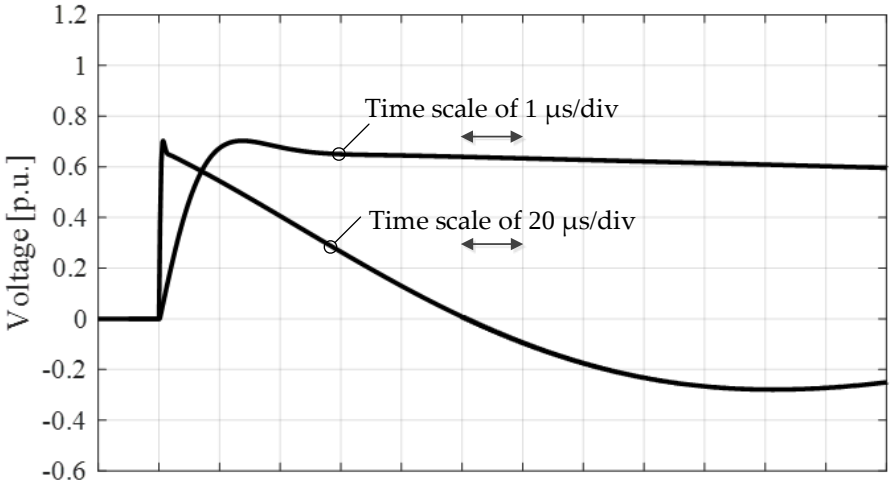

Figure 8. Generated waveform of Case 1 in Table 4 and by the proposed approach.

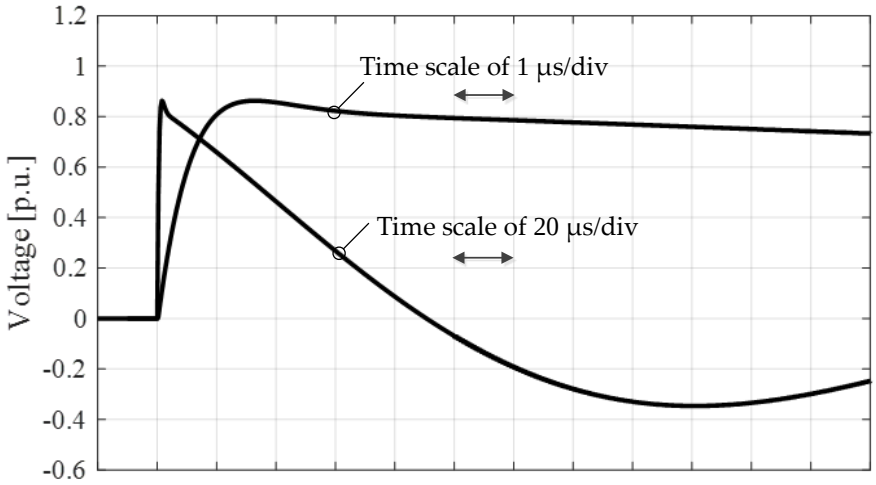

Figure 9. Generated waveform of Case 3 in Table 4 and by the proposed approach.

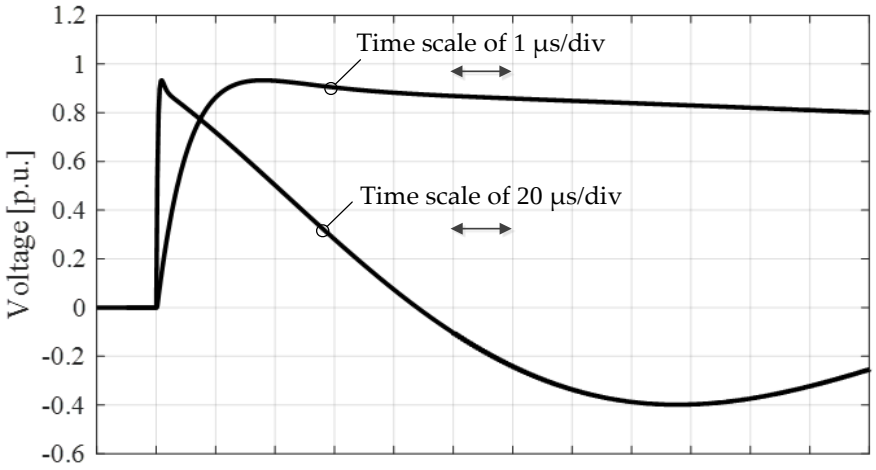

Figure 10. Generated waveform of Case 5 in Table 4 and by the proposed approach.

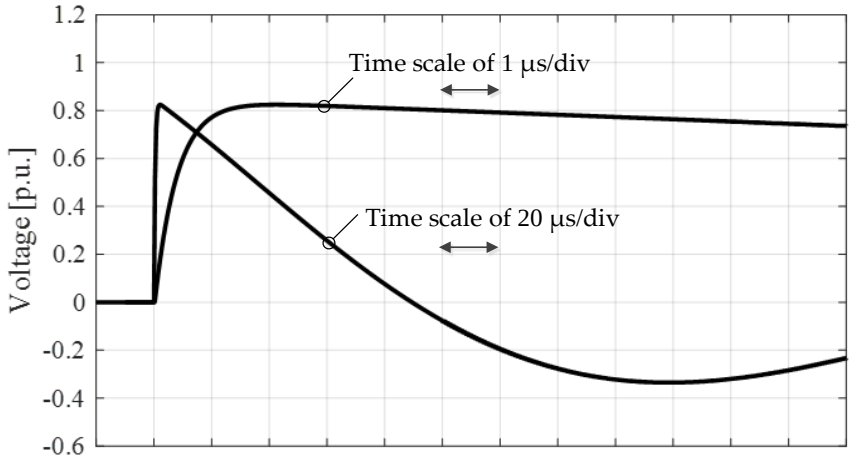

Figure 11. Generated waveform of Case 7 in Table 4 and by the proposed approach.

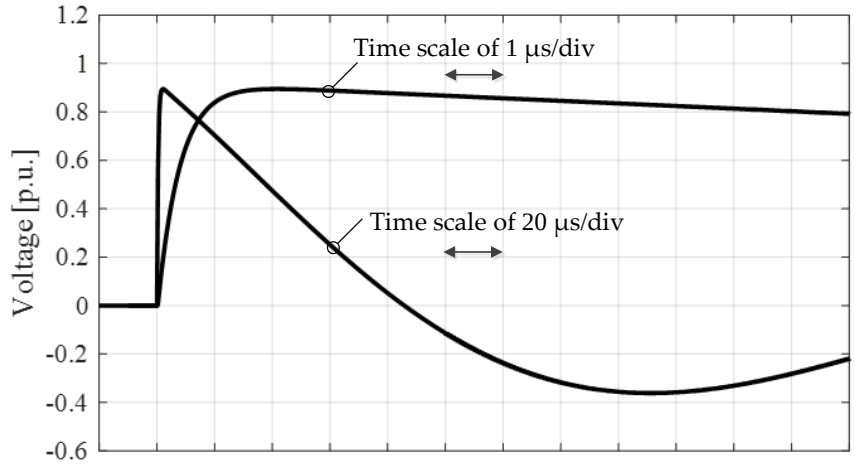

Figure 12. Generated waveform of Case 9 in Table 4 and by the proposed approach.

In the first experiment (Case 12), the charging voltage was set to 6.1 kV to obtain the peak voltage of about 6 kV. A 1-nF voltage divider and a 3-nF capacitor were connected across the load to obtain the total load capacitance of 4 nF. With the proposed approach, the selected circuit parameters of C_s, R_d, L_d, R_p and R_e were 2 μF, 120 Ω, 100 μH, 300 Ω and 60 Ω, respectively. In the second experiment (Case 13), the charging voltage was set to 33 kV to obtain the peak voltage of about 30 kV. A 1-nF voltage divider and a 7-nF capacitor were connected across the load to obtain the total load capacitance of 8 nF. With the proposed approach, the selected circuit parameters of C_s, R_d, L_d, R_p and R_e were 3 μF 50 Ω, 100 μH, 200 Ω and 35 Ω, respectively. The circuit parameters fo the experiments and simulation are shown in Table 8, the comparison of the generated waveforms are presented in Figures 13 and 14 and the waveform parameters are shown in Table 9. It was found that the simulation and experimental waveforms agree well.

Table 8. Circuit component parameters of the generated waveforms in the example cases.

Case No.		Circuit Component Parameters						
		L_L (mH)	C_b (nF)	C_s (μF)	R_d (Ω)	L_d (mH)	R_p (Ω)	R_e (Ω)
12	Simulation	2.013	4.0	2.0	121.26	0.1	314.45	57.06
	Experiment	2.013	4.0	2.0	120.00	0.1	300.00	60.00
13	Simulation	1.308	8.0	3.0	50.92	0.1	205.70	35.80
	Experiment	1.308	8.0	3.0	50.00	0.1	200.00	35.00

Table 9. Circuit and waveform parameters of the generated waveforms in the example cases.

Case No.		Waveform Parameters				
		Efficiency (%)	T_1 (μs)	T_2 (μs)	Overshoot (%)	Undershoot (%)
12	Simulation	99.02	1.16	40.79	+1.65	40.36
	Experiment	97.48	1.14	40.49	+1.49	39.31
13	Simulation	92.35	1.16	41.71	−2.43	40.66
	Experiment	91.80	1.14	41.55	−2.04	40.05

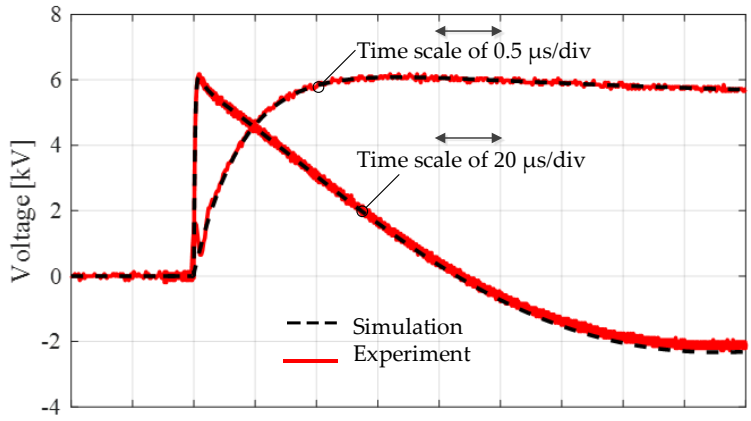

Figure 13. Comparison of the simulation and experimental waveforms in Case 12.

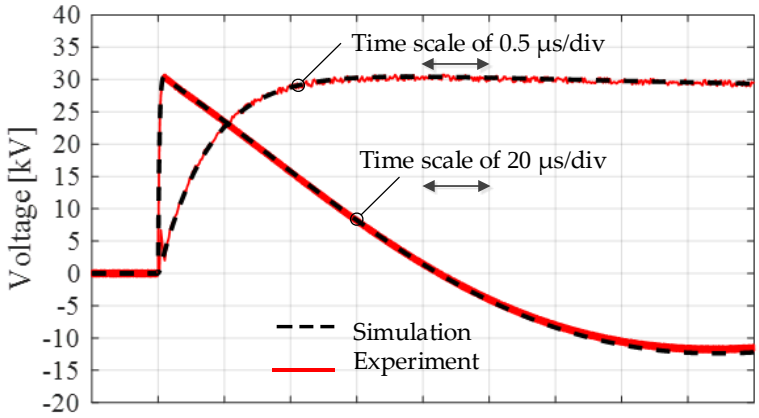

Figure 14. Comparison of the simulation and experimental waveforms in Case 13.

4. Conclusions

The limitation of using the Glaninger circuit with Feser parameter selection equation when dealing with a low inductance load is noted and discussed. To provide an accurate impulse voltage waveform according to the standard requirement, adjustment of the circuit component parameters of the Glaninger circuit is required. A system parameter identification based on an artificial neural network algorithm is successfully adopted for selection of the suitable circuit components depending on the circuit load parameters, load inductance and capacitance. It was found that the approach for circuit parameter selection of the impulse voltage generation circuit proposed in this paper can be employed with low inductance load conditions. Using the proposed approach, the designed circuit generated the impulse voltage waveform with less distortion, an efficiency higher than 60% and an undershoot voltage of about 40%. It was found that the proposed approach in parameters selection of the generation circuit can function well in the impulse voltage test of a low inductance load with the load inductance from 400 μH to 4 mH and with the load capacitance from 1 to 10 nF.

Author Contributions: Conceptualization, P.T. and P.Y.; Methodology, P.T., K.K. and P.Y.; Software, P.T., K.K. and P.Y.; Validation, P.T. and P.Y.; Formal analysis, P.T. and P.Y.; Investigation, P.T., P.Y. and A.K.; Writing-original draft preparation, P.T. and P.Y.; Writing-review and editing, P.T., P.Y. and A.K.; Supervision, P.Y. All authors have read and agreed to the published version of the manuscript.

Funding: This work was financially supported by Research and Researchers for Industries (RRi), the Thailand Research Fund No. PHD57I0035.

Acknowledgments: This work was financially supported by Research and Researchers for Industries (RRi), the Thailand Research Fund No. PHD57I0035. The authors also would like to thank Sakda Maneerot of LAMOOL TRANSFORMERS and TESLA POWER Co Ltd. for his technical advices.

Conflicts of Interest: TThe authors declare no conflict of interest.

References

1. IEC 60060-1. *High-Voltage Test Techniques. Part 1: General Definitions and Test Requirements*, 3rd ed.; International Electrotechnical Commission (IEC): Geneva, Switzerland, 2010.
2. IEEE Standard 4TM-2013. *IEEE Standard for High-Voltage Testing Techniques*; Institute of Electrical and Electronics Engineers (IEEE): Piscataway, NJ, USA, 2013.
3. Kuffel, E.; Zaengl, W.S.; Kuffel, J. *High Voltage Engineering: Fundamentals*, 2nd ed.; Newnes: Oxford, UK, 2000.
4. IEC 60076-1. *Power Transformer. Part 1: General*, 3rd ed.; International Electrotechnical Commission (IEC): Geneva, Switzerland, 2011.
5. IEC 60076-3. *Power Transformer. Part 3: Insulation Level, Dielectric Tests and External Clearances in Air*, 3rd ed.; International Electrotechnical Commission (IEC): Geneva, Switzerland, 2013.
6. IEC 60076-4. *Power Transformer. Part 4: Guide to the Lightning Impulse and Switching Impulse Testing—Power Transformer and Reactors*, 1st ed.; International Electrotechnical Commission (IEC): Geneva, Switzerland, 2002.
7. Karthikeyan, B.; Rajesh, R.; Balasubramanian, M.; Saravanan, S. Experimental investigations on IEC suggested methods for improving waveshape during impulse voltage testing. In Proceedings of the 2006 IEEE 8th International Conference on Properties & Applications of Dielectric Materials, Bali, Indonesia, 26–30 June 2006.
8. Glaninger, P. Impulse testing of low inductance electrical equipment. In Proceedings of the 2nd International Symposium on High Voltage Technology, Zurich, Switzerland, 9–13 September 1975; pp. 140–144.
9. Schrader, W.; Schufft, W. *Impulse Voltage Test of Power Transformers*; Paper No. 13; HV Technologies, Inc.: Manassas, VA, USA, 2000.
10. IEC 61083-2. *Instruments and Software Used for Measurement in High-Voltage and High Current Tests—Part 2: Requirements for Software for Tests with Impulse Voltages and Currents*, 2nd ed.; International Electrotechnical Commission (IEC): Geneva, Switzerland, 2013.
11. Pattanadech, N.; Yutthagowith, P. Fast curve fitting algorithm for parameter evaluation in lightning impulse test technique. *IEEE Trans. Dielectr. Electr. Insul.* **2015**, *22*, 2931–2936. [CrossRef]
12. Yutthagowith, P.; Pattanadech, N. Improved least-square prony analysis technique for parameter evaluation of lightning impulse voltage and current. *IEEE Trans. Power Deliv.* **2016**, *31*, 271–277. [CrossRef]
13. Feser, K. Circuit design of impulse generators for the lightning impulse voltage testing of transformers. *Bull. SEV/VSE Bd* **1978**. Available online: www.haefely.com (accessed on 15 November 2019).
14. Mirzaei, H. A Simple Fast and Accurate Simulation Method for Power Transformer Lightning Impulse Test. *IEEE Trans. Power Deliv.* **2019**, *33*, 1151–1160. [CrossRef]
15. Mirzaei, H.; Bayat, F.; Miralikhani, K. A Semi-Analytic Approach for Determining Marx Generator Optimum Set-up during Power Transformers Factory Test. *IEEE Trans. Power Deliv. (Early Access)* **2020**. [CrossRef]
16. Yutthagowith, P.; Tuethong, P.; Pattanadech, N. Effective circuit parameter determination in lightning impulse voltage tests of air core inductors. In Proceedings of the 12th IET International Conference on AC and DC Power Transmission, Beijing, China, 28–29 May 2016.
17. Demuth, H.; Beale, M. *Neural Network Toolbox User's Guide*; The Mathworks Inc.: Natick, MA, USA, 1992.